magnetochemistry

Article

Preparation and Characterization of BXFO High-Entropy Oxides

Saba Aziz [1,*], Anna Grazia Monteduro [1], Ritu Rawat [1], Silvia Rizzato [1], Angelo Leo [1], Shahid Khalid [2] and Giuseppe Maruccio [1,*]

[1] Omnics Research Group, Department of Mathematics and Physics, University of Salento, CNR-Institute of Nanotechnology, INFN Sezione di Lecce, Via per Monteroni, 73100 Lecce, Italy; annagrazia.monteduro@unisalento.it (A.G.M.); ritu.rawat@unisalento.it (R.R.); silvia.rizzato@unisalento.it (S.R.); angelo.leo@unisalento.it (A.L.)

[2] Department of Materials Science, University of Milano Bicocca, 20126 Milan, Italy; shahid.khalid@unimib.it

* Correspondence: saba.aziz@unisalento.it (S.A.); giuseppe.maruccio@unisalento.it (G.M.)

Abstract: Increasing demand for functional materials crucial for advancing new technologies has motivated significant scientific and industrial research efforts. High-entropy materials (HEMs), with tunable properties, are gaining attention for their use in high-frequency transformers, microwave devices, multiferroics, and high-density magnetic memory components. The initial exploration of HEMs started with high-entropy alloys (HASs), such as CrMnFeCoNi, CuCoNiCrAlxFe, and AlCoCrTiZn and paved the way for a multitude of HEM variations, including oxides, oxyfluorides, borides, carbides, nitrides, sulfides, and phosphides. In this study, we fabricated the high-entropy oxide (HEO) compound $Bi_{0.5}La_{0.1}In_{0.1}Y_{0.1}Nd_{0.1}Gd_{0.1}FeO_3$ through the solid-state synthesis method. Magnetic measurements at 300 K show ferromagnetic behavior with significant coercivity. At the same time, this novel composition exhibits excellent dielectric properties and shows potential for electronic applications demonstrating that a high-entropy approach can expand the compositional range of rare earth multiferroics and improve the multifunctional properties in multiferroic applications.

Keywords: multi-doping; multiferroics; high-entropy oxides; bismuth ferrite; magnetization

Citation: Aziz, S.; Monteduro, A.G.; Rawat, R.; Rizzato, S.; Leo, A.; Khalid, S.; Maruccio, G. Preparation and Characterization of BXFO High-Entropy Oxides. *Magnetochemistry* **2024**, *10*, 60. https://doi.org/10.3390/magnetochemistry10080060

Academic Editor: Lotfi Bessais

Received: 9 July 2024
Revised: 7 August 2024
Accepted: 14 August 2024
Published: 15 August 2024

1. Introduction

Doping has long been recognized as a powerful tool for tailoring the structure and properties of functional materials, including ceramics, offering a pathway to enhance their performance in various applications [1,2]. The effectiveness of doped materials is influenced by factors such as the type, concentration, and number of dopants, with the latter being particularly crucial for exploring a broad compositional space to achieve desired properties [1]. Historically, the incorporation of dopants into a single compound was limited by a perceived barrier, typically involving two or three dopants within a lattice structure [3,4]. However, in 2015, Rost et al. introduced a groundbreaking concept known as high-entropy ceramics (HECs), which incorporate five or more cations in at least one sublattice and rely on entropy rather than enthalpy to stabilize the material in a single phase [3], thereby expanding the compositional landscape beyond traditional doping paradigms. The phenomenon involves the mixing of various oxides rather than doping because all of the cations have to be in equimolecular ratio according to the notion. Since then, the emergence of high-entropy ceramics sparked significant interest in the pursuit of novel functional materials, leading to intensive research efforts over the past five years. Studies in this area have demonstrated the efficacy of compositional disorder, or cationic disorder, in tailoring the functional properties of materials [3,5,6]. Recent developments by Wright et al. expanded the concept of high-entropy ceramics to encompass compositionally complex ceramics (CCCs), opening up new avenues for exploring non-equimolecular compositions [7]. By incorporating five or more cations in a single lattice site, CCCs offer the potential for structural stabilization and enhanced functionalities even at low- and medium-entropy regions.

$BiFeO_3$(BFO) multiferroic is a highly promising material due to its multifunctional properties, including electric and antiferromagnetic behavior, making it suitable for various technological applications [8]. Despite its potentials, BFO suffers from drawbacks such as high leakage current and difficulty in synthesis, limiting its practical utility [8,9]. Doping studies have shown promise in addressing these challenges, with substitutions at both A- and B-sites leading to improvements in magnetic and electrical properties [10–12]. Aungkan Sen et al. broaden the application of the CCCs concept to perovskite ABO_3-type oxides, by exploring the effects of multi-principal cation doping on $BiFeO_3$, with a particular focus on the incorporation of five different cations (Mo^{6+}, Ti^{4+}, Ce^{4+}, Ni^{2+}, and Zr^{4+}) at B-sites (Fe-sites). In their study, they observe the structural and functional changes induced by compositional disorder by systematically varying the dopant composition [13]. Our research builds upon these findings by exploring the effects of multi-doping on BFO, with a particular focus on the incorporation of five different cations from (La^{3+}, In^{3+}, Y^{3+}, Nd^{3+}, Gd^{3+}) at A-sites (Bi-sites). By interpreting the relationship between compositional complexity and material properties through characterization techniques, such as X-ray diffraction, along with electric and magnetic measurements, we aim to explore the potential of multi-doping in perovskite oxides and its implications for the design of advanced functional materials.

2. Materials and Methods

2.1. Materials and Synthesis

The $Bi_{0.5}La_{0.1}In_{0.1}Y_{0.1}Nd_{0.1}Gd_{0.1}FeO_3$ (BXFO), (X = La, In, Y, Nd, Gd), high-entropy oxides and single-component oxide (BFO) were fabricated by the conventional solid-state method with high-purity Bi_2O_3, La_2O_3, In_2O_3, Y_2O_3, Nd_2O_3, Gd_2O_3, and Fe_2O_3 as starting powders. BXFO was prepared using the molar ratio of the precursors (Bi_2O_3:Y_2O_3:In_2O_3:La_2O_3:Nd_2O_3:Gd_2O_3:Fe_2O_3 = 0.5:0.1:0.1:0.1:0.1:0.1:1). For each sample, powders were weighed according to the stoichiometric formula of each element. After weighing the reagent powders with a precision balance, they are transferred to the grinder's agate mortar (SFM-8 Agate Mortar Grinder), adding isopropanol to improve the mixing process and thus the homogeneity of the compound, which at this stage is mixed for 6 h at rate of 80–90 rpm. At the end of the mixing process, the powders were air-dried and then poured into an alumina crucible for the heat treatment (calcination). A cylindrical alumina furnace, model GSL—1700X was used, and the samples were heated at different temperatures to study the effect of temperature on the structure and crystallinity. Calcination temperature ranged from 830 to 1200 °C for 3h at 5 °C min^{-1}. The synthesized powders were then pressed into a 16 mm diameter pellet under a uniaxial pressure of 10 kN for 10 min, followed by sintering at 700 °C for 2 h at 5 °C·min^{-1}; a Veeco Dektak 6M Stylus Profilometer was used to measure the thickness. A schematic representation of the various steps involved during the synthesis process is shown in Figure 1.

2.2. Characterization

The crystal structures of the BXFO and BFO were investigated by an X-ray diffractometer (X'PERT PRO PANalytical diffractometer) equipped with Cu Kα radiation from 20° to 70° at a scan rate of 8° min^{-1}. X-ray diffraction (XRD) patterns were fitted by the Rietveld method using the software FullProf. suite (5.10) version: January-2023. For dielectric measurements, pellets were polished with sandpaper into smooth, parallel surfaces with a thickness of approximately 400 microns. After polishing, a silver adhesive was used to make electric contacts on the top and bottom surfaces, followed by repolishing to avoid the effects of any contamination on the measurements. The relationship between the dielectric properties and the frequency of each sample was measured by an LCR precision meter model E4980A (Agilent Technologies Inc., Santa Clara, CA, USA), which allows one to measure the capacitance (C) and the dissipation factor (Tgδ or D), by applying a sinusoidal signal with a variable frequency (V_{AC}). Measurements were conducted by applying a V_{AC}

of 500 mV in a frequency range of 100 Hz to 1 MHz. The dielectric constant was calculated by using the following equation:

$$C = \frac{\epsilon \epsilon_o S}{d}$$

where the S is the area of the capacitor's plate, d is the thickness of the capacitor, and ϵ_o is the electric constant (8.85×10^{-12} C^2/Nm^2).

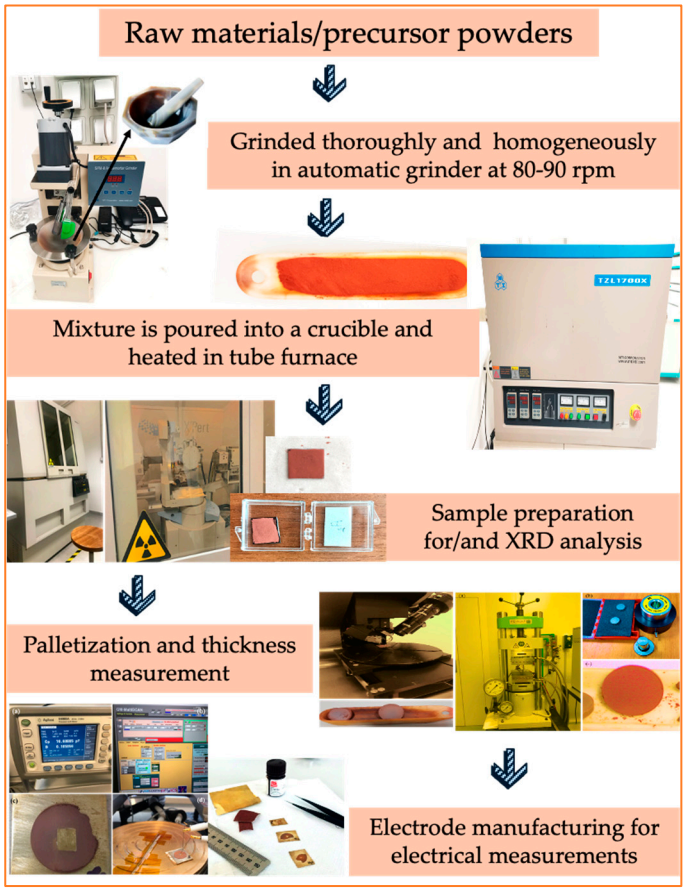

Figure 1. Schematic of the synthesis method adopted for the preparation of investigated samples.

A vibrating sample magnetometer (VSM, Cryogenic Ltd., London, UK) was used to measure the magnetic hysteresis loops at room temperature in an applied field of 0.5 T.

3. Results and Discussion

3.1. Structural Characterization

Figure 2 illustrates the structural characterization of the pristine BFO, and the multi-doped sample calcined at two different temperatures (830 °C and 1200 °C). The recorded spectra were analyzed using MATCH! software version 3.16 Build 288, performing a comparative analysis of BXFO and BFO samples. The objective was to identify any changes in the crystallographic phase of the multi-doped sample such as if there is any alteration in peak positions, intensities, and/or patterns, which could provide valuable insights into the structural modifications induced by the doping process and subsequent calcination at different temperatures. This is crucial for understanding how the incorporation of dopants influences the overall crystal structure and phase purity of the material, thus guiding further optimization strategies.

From the spectra, it is observed that the BXFO sample calcinated at 830 °C lacks an anticipated crystallographic order typical of perovskite-type $BiFeO_3$. Instead, it exhibits a presence of several impure phases and unreacted element peaks, indicating incomplete reaction at this temperature. The formation of impurities and unreacted components

suggests and highlights the critical need for control over calcination conditions to achieve desired structure. BXFO calcinated at 1200 °C represents a clear crystallographic order, indicating a more complete reaction and phase formation process. However, despite this improvement, minor peaks of spurious phase, compatible with a sillenite type, are present. The percentage of pure as well as impure BFO phase composition (in volume %) along with unreacted elements are elaborated in Table 1. The presence of these secondary phases, while common in BFO, highlights the complexity of the doping and calcination processes, as well as the challenges in achieving high phase purity in multi-doped materials. Moreover, we also observed subtle shifts in reflection patterns in the XRD spectra highlighted in Figure 2b. These shifts indicate a slight variation in the unit cell structure of $BiFeO_3$, potentially stemming from lattice distortions or modifications induced by the doping and calcination processes [14,15].

Table 1. Phase composition of pure BFO phase as well as other impure phases present and values of dialectic and conductivity responses at min. and max. frequencies.

Samples	Phase Composition of $BiFeO_3$ and Other Impure Phases Present (%)						Electric Responses at Room Temperature							
							ε'		ε''		$Tg\delta$		σ (S·cm^{-1})	
	$BiFeO_3$	$Bi_{25}FeO_{40}$	$Bi_2Fe_4O_9$	Gd_2O_3	Y_2O_3	In_2O_3	100 Hz	1 MHz	100 Hz	1 MHz	100 Hz	1 MHz	100 Hz	1 MHz
BFO	88.7	11.3	-	-	-	-	460	100	112	30	0.3	0.21	6.5×10^{-7}	9.9×10^{-4}
BXFO-830 °C	12	-	49.8	16.1	11.1	11	210	85	73	30	0.3	0.4	4.3×10^{-7}	0.002
BXFO-1200°C	72.5	12.9	14.6	-	-	-	3.8k	634	6k	30	1.7	0.04	3.3×10^{-5}	0.002

The concept of entropy stabilization is rooted in the enhancement of configurational entropy (ΔS_{conf}) for stabilizing a single-phase crystal structure. This is achieved by introducing a greater number of elements randomly distributed across lattice sites. This entropy stabilization can appear when the entropy-dependent term ($T\Delta S_{mix}$) in the Gibbs–Helmholtz equation (Equation (1)) compensates for the mixing enthalpy (ΔH_{mix}), which arises when different elements are mixed.

$$\Delta G_{mix} = \Delta H_{mix} - T\Delta S_{mix} \quad (1)$$

Since in this case

$$\Delta G_{mix} = -T\Delta S_{mix} \quad (2)$$

it can be considered that the entropy acts as the driving force for single-phase stabilization, and

$$\Delta S_{conf} = \Delta S_{mix} = -R[(\sum_{a=1}^{i} x_a \ln x_a)_{A-site} + (\sum_{b=1}^{i} x_b \ln x_b)_{B-site} + 3(\sum_{o=1}^{i} x_o \ln x_o)_{O-site}] \quad (3)$$

where ΔS_{mix} is the mixing entropy, also called configurational entropy (ΔS_{conf}); R is the gas constant; x_a, x_b, and x_o are the mole fractions of each component present in each site (A-site, B-site, and O-site) of the sublattice in the solid solution, respectively, and ln is the natural logarithm. The x_a, x_b, and x_o values can be calculated based on the stoichiometry of the material.

In HEOs, the incorporation of additional elements results in an increase in ΔS_{conf}, with the maximum value attained when all elements are present in equiatomic proportions. When a material's configurational entropy $\Delta S_{conf} \geq 1.5$ R, it can be classified as a high-entropy material, indicating a substantial rise in entropy owing to the addition of multiple elements. However, it is essential to note that achieving a single phase solely based on $\Delta S_{conf} \geq 1.5$ R is not guaranteed, as other factors such as ΔH_{mix} must also be considered [16].

In our case, the mole fractions of Bi, La, In, Y, Nd, Gd, and Fe in the overall composition are defined as follows:

$$X_{Bi} = 0.5,\ X_{La} = X_{In} = X_{Y} = X_{Nd} = X_{Gd} = 0.1,\ \text{and}\ X_{Fe} = 1$$

This compositional complexity contributes to an increase in configurational entropy (ΔS_{conf}), which quantifies the disorder or randomness in the arrangement of atoms within the crystal lattice. By substituting these values into the formula to calculate the mixing/configurational entropy, $\Delta S_{mix}/\Delta S_{conf}$ for BXFO equals 1.5R (0.012471 kJ mol^{-1} K^{-1}) due to the incorporated elements into the A-site. Empirical classification designates materials with ΔS_{conf} greater than or equal to 1.5R as "high entropy" [17]. This classification underscores the significant disorder present in the atomic arrangement of high-entropy materials, indicating a departure from traditional crystalline structures characterized by a single dominant element.

In the context of XRD spectra analysis, the presence of impurities and unreacted components, especially at lower calcination temperatures, poses challenges in achieving high-entropy materials with sufficient configurational entropy to stabilize a single-phase crystal structure. This emphasizes the importance of precise control over synthesis conditions for acquiring the desired material properties, particularly with respect to high-entropy systems.

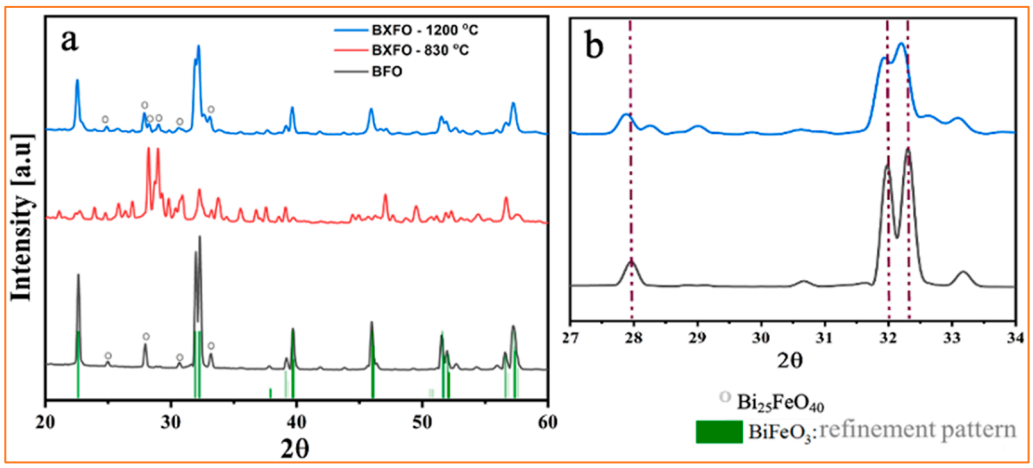

Figure 2. (**a**) A comparison between the XRD spectra of the BXFO sample calcinated at (830 °C and 1200 °C) with the spectrum of the pristine BFO and (**b**) indication of peak shift of BXFO-1200 °C with respect to pristine BFO.

3.2. Dielectric Properties

Figure 3 compares the frequency-dependent (100 Hz–1 MHz) dielectric responses and conductivities of the samples analyzed at room temperature (RT). The value of the dielectric constant varies with the frequency of an electric field. In the lower frequency region, the response is high, while it declines with the increase in frequency for all the samples. At 100 Hz, the permittivity value of BXFO-830 °C ceramic is 185, with a tangent loss of 0.38, while for BXFO-1200 °C, the permittivity rises to 3760 with a tangent loss of approximately 1.7. Pristine BFO ceramic shows a permittivity of 485 with a tangent loss of 0.2. Detailed parameter values at 100 Hz and 1 MHz are presented in Table 1.

Figure 3a,b show the comparison of dielectric constant and dielectric loss values as a function of frequency. In dielectric materials, especially ceramics, the observed behavior at lower frequencies is often attributed to both relaxation and space charge polarization, where charges accumulate at interfaces or within the material's structure, altering its dielectric properties. As frequency increases, influence of relaxation polarization's decreases, leaving displacement polarization to stabilize the dielectric constant, and the dielectric constant settles into a steady state, reflecting the Maxwell–Wagner and Koop models. These

models explain how conductive particles separated by insulating boundaries affect polarization dynamics: at low frequencies, high resistance at grain boundaries causes space charge polarization, while higher frequencies lead to reduced polarization due to electron mobility changes [18–21].

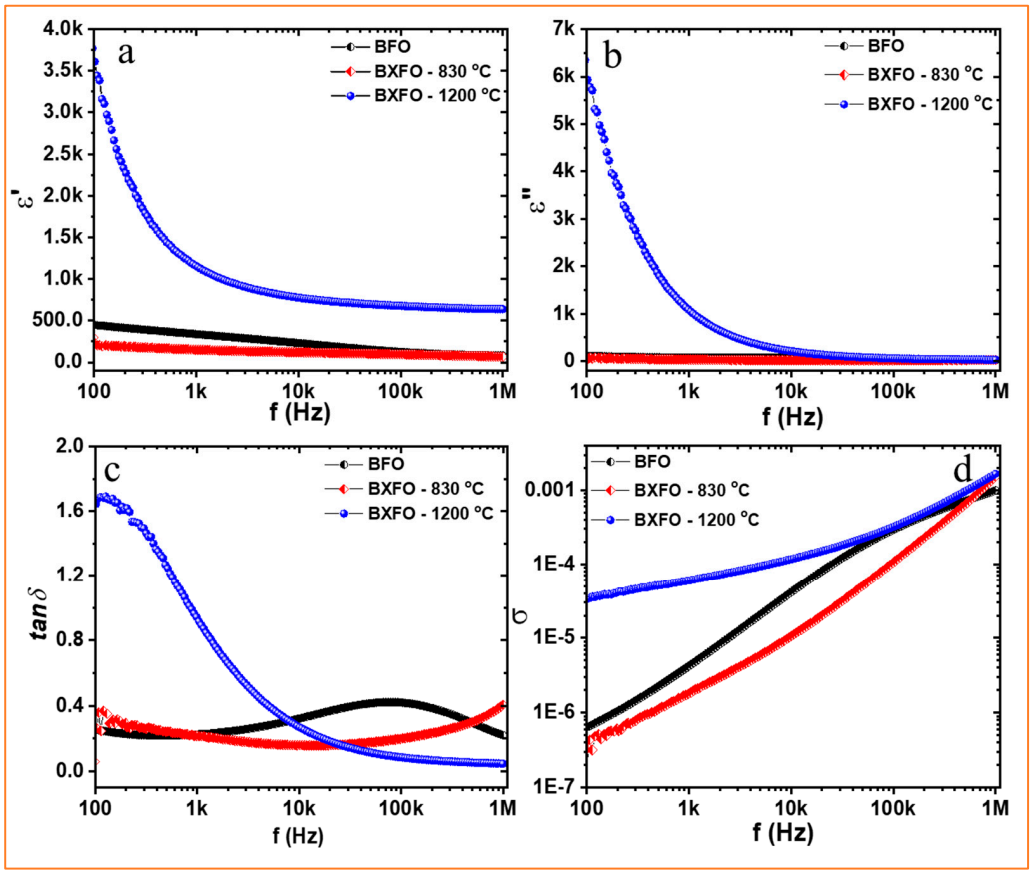

Figure 3. A comparison of the electrical properties of the samples BXFO-830 °C and BXFO-1200 °C with pristine BFO: (**a**) the real part of electrical permittivity as a function of frequency and (**b**) the imaginary part of electrical permittivity (dielectric losses). (**c**) A graph of the trend of the dissipation factor with respect to the frequency for all the analyzed samples (**d**) and conductivity values as a function of frequency.

The increase in tangent loss observed in BXFO-1200 °C ceramics (Figure 3c) compared to pristine BFO may result from various factors, including grain boundary effects, dopant incorporation, or defect-related relaxation processes [22–24]. The trade-off between dielectric constant and losses, influenced by processing parameters and dopant selection, may contribute to these elevated losses. For example, the presence of low-valence ions can induce oxygen vacancies in the lattice, leading to heightened space charge in the ceramics and higher dielectric losses in the low-frequency range due to space charge polarization [18–20].

The higher conductivity of BXFO-1200 °C, as depicted in Figure 3d, can be attributed to multiple factors, particularly in complex systems like this with multi-dopants. Elevated conductivity suggests an abundance of charge carriers within the material, likely due to dopants, defects, or impurities, which facilitate electric current conduction. However, this increased concentration of charge carriers leads to more frequent collisions with lattice imperfections, dissipating energy as heat and resulting in higher dielectric losses. Moreover, conductivity may exacerbate dielectric relaxation processes within the material, involving the realignment of electric dipoles in response to an external electric field, accompanied by energy dissipation. As charge carriers influence dielectric relaxation dynamics, materials

with high conductivity tend to exhibit higher dielectric losses due to an increased interaction between charge carriers and the lattice structure [25].

3.3. Magnetic Properties

The room temperature magnetic analysis conducted through VSM measurements provided an insight into the magnetic behavior of the samples; this is shown in Figure 4. Hysteresis loops (M-H loops) of magnetization versus applied magnetic field were recorded up to 0.5 T (5k Oe), and parameters such as magnetization and coercivity were extracted from these curves. The recorded hysteresis loops revealed distinct characteristics for each sample, indicating variations in magnetization and coercivity parameters and the values obtained for each sample as given in Table 2. The spin structure of BFO in its pure form is G-type AFM. The spin structure is also modulated by Dzyaloshinskii–Moriya interactions (DMI) which establish both spin-canting and a long-period spin cycloid of length ~64 nm. A small residual magnetic moment is observed in BFO due to canted Fe^{3+} (as also observed in our case; see Figure 4); however, the FM phase is suppressed. The magnetization can be improved if the grain size is decreased below 62 nm. There is also a possibility of observing FM behavior due to the presence of magnetic impurities such as Fe_2O_3. However, we can rule out both of these possibilities for BXFO-830 °C and BXFO-1200 °C, as the grain size is in the μm range and the XRD does not indicate the presence of a Fe_2O_3 impurity phase. The magnetic behavior observed is hence the intrinsic nature of the grown samples [8]. In BXFO-830 °C, as the presence of a high amount of impurities and defects are more prevalent; it influences the magnetization as well. The higher coercivity is a consequence of higher impurity phase. It is more apparent as when BXFO is calcinated at 1200 °C; the coercivity decreases significantly as the percentage of impurity phases decreases.

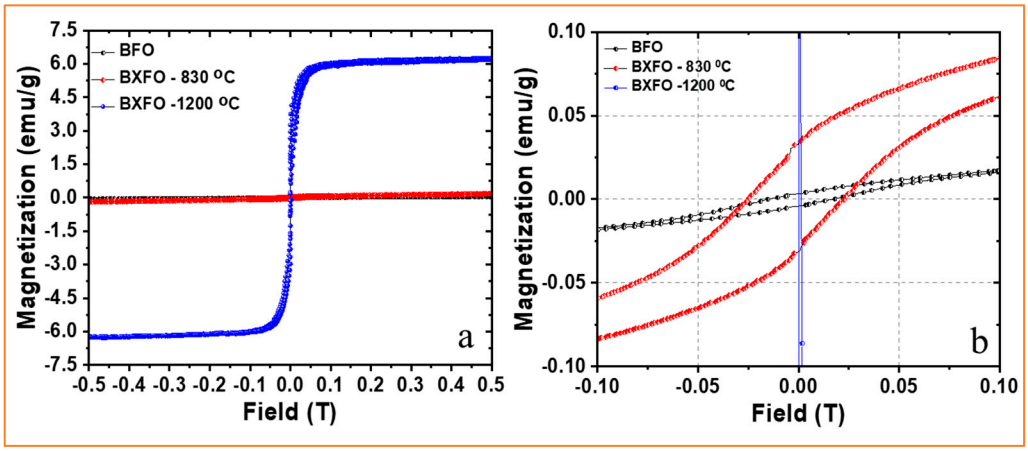

Figure 4. (**a**) M-H hysteresis loops of BXFO-830 °C and BXFO-1200 °C in comparison with pristine BFO ceramics; (**b**) magnified hysteresis of (**a**).

Table 2. Values of saturation magnetization, remanent magnetization, and coercivity.

Samples	Magnetization Values		
	$Ms\ (\frac{emu}{g})$	$Mr\ (\frac{emu}{g})$	$Hc\ (T)$
BFO	0.05	0.003	0.015
BXFO-830 °C	0.176	0.04	0.02
BXFO-1200 °C	5.9	4.1	0.002

BXFO calcinated at 1200 °C shows higher saturation magnetization (Ms = 5.9 emu/g) value as well, due to the distribution of substituent cations [6]. The enhancement in magnetic behavior due doping at the Bi-site leads is primarily due to the modification in the Fe-O-Fe bond angle and bond length [26]. La-doping may contribute in coercivity

due to magneto-crystalline anisotropy. Additionally, Nd and Gd doping will enhance magnetization. It is important to understand the individual contribution of these types of doping on BFO structurally, magnetically, and electrically. In order to understand the indirect super-exchange interactions between the substituted ions and oxygen (X–O–X), it is important to know exactly how these ions are distributed within the crystal structure. Since XRD alone is insufficient, further studies, including Mössbauer spectroscopy and neutron diffraction, could contribute to a better understanding of these interactions. Additionally, the high-entropy nature of the material, characterized by a complex arrangement of elements in equiatomic proportions, can introduce magnetic disorder and complexity, further impacting its magnetic behavior.

4. Conclusions and Prospects

BXFO samples, doped at the A-site and calcined at 1200 °C, were synthesized via the solid-state method. X-ray diffraction patterns confirmed the formation of a perovskite-type bismuth ferrite phase with an R3C crystal structure. The structural, electrical, and magnetization outcomes of the analyzed samples, with respect to pristine BFO, highlight how multi-doping and high-entropy characteristics influence these properties. Looking ahead, further investigation into the role of specific dopants and their concentrations on the magnetic properties of high-entropy oxides like BXFO could provide valuable insights to fine-tune such materials while minimizing losses, which would be beneficial for applications. Furthermore, studying the impact of different doping concentrations could offer a deeper understanding of the fundamental mechanisms and help optimize material performance for targeted applications.

Author Contributions: Conceptualization: G.M. and S.A.; methodology: S.R. and A.G.M.; formal analysis: S.R. and R.R.; investigation: S.A.; resources: G.M. and A.G.M.; data curation: S.A. and A.L.; writing—original draft: S.A.; supervision: G.M. and A.G.M.; writing—review and editing: all authors. All authors have read and agreed to the published version of the manuscript.

Funding: This research was partially funded by (1) UE-H2020-INFRADEV-2018-2020 project ISABEL (Improving the sustainability of the European Magnetic Field Laboratory), grant no. 871106; (2) EU-EIT-RAW Materials, RIS Capacity Building project PARSIVAL (pv PAnels Recycling to create SIlicon VALue chain), grant no. 22001; (3) Italian PNRR—M4C2I3.1 project IRIS (Innovative Research Infrastructure on applied Superconductivity), grant no. IR0000003; (4) Italian MUR-PRIN Project MoRe-SPIN (Tailoring magneto-electric and magneto-elastic couplings in artificial heterostructures for multifunctional devices and reconfigurable sensors): prot. 2022BZYBWM; (5) Italian MUR-PRIN Project GINEVRA (Gas sensors based on engINeered hybrid nanomaterials for Volatilomics, enviRonmentAl and food monitoring), prot. 2022BZYBWM; (6) Puglia Region—Education and University Section 24 February 2020, n. 20—POR Puglia FESR ESF 2014-2020—Axis X—Action 10.4 "Interventions aimed at promoting research and university education". Approval of public notice no. 1/FSE/2020—POR PUGLIA FESR-FSE 2014/2020.

Data Availability Statement: The original contributions presented in the study are included in the article, further inquiries can be directed to the corresponding authors.

Conflicts of Interest: The authors declare no conflicts of interest.

References

1. Wrzesińska, A.; Khort, A.; Witkowski, M.; Szczytko, J.; Ryl, J.; Gurgul, J.; Kharitonov, D.S.; Łątka, K.; Szumiata, T.; Wypych-Puszkarz, A. Structural, electrical, and magnetic study of La-, Eu-, and Er- doped bismuth ferrite nanomaterials obtained by solution combustion synthesis. *Sci. Rep.* **2021**, *11*, 22746. [CrossRef]
2. Verma, V.; Beniwal, A.; Ohlan, A.; Tripathi, R. Structural, magnetic and ferroelectric properties of Pr doped multiferroics bismuth ferrites. *J. Magn. Magn. Mater.* **2015**, *394*, 385–390. [CrossRef]
3. Rost, C.M.; Sachet, E.; Borman, T.; Moballegh, A.; Dickey, E.C.; Hou, D.; Jones, J.L.; Curtarolo, S.; Maria, J.P. Entropy-stabilized oxides. *Nat. Commun.* **2015**, *6*, 8485. [CrossRef]
4. Salian, A.; Pujar, P.; Vardhan, R.V.; Cho, H.; Kim, S.; Mandal, S. Evolution of High Dielectric Permittivity in Low-Temperature Solution Combustion-Processed Phase-Pure High Entropy Oxide (CoMnNiFeCr)O for Thin Film Transistors. *ACS Appl. Electron. Mater.* **2023**, *5*, 2608–2623. [CrossRef]

5. Sarkar, A.; Wang, Q.; Schiele, A.; Chellali, M.R.; Bhattacharya, S.S.; Wang, D.; Brezesinski, T.; Hahn, H.; Velasco, L.; Breitung, B. High-Entropy Oxides: Fundamental Aspects and Electrochemical Properties. *Adv. Mater.* **2019**, *31*, 1806236. [CrossRef] [PubMed]
6. Zhivulin, V.E.; Trofimov, E.A.; Zaitseva, O.V.; Sherstyuk, D.P.; Cherkasova, N.A.; Taskaev, S.V.; Vinnik, D.A.; Alekhina, Y.A.; Perov, N.S.; Naidu, K.C.B.; et al. Preparation, phase stability, and magnetization behavior of high entropy hexaferrites. *IScience* **2023**, *26*, 107077. [CrossRef]
7. Wright, A.J.; Wang, Q.; Huang, C.; Nieto, A.; Chen, R.; Luo, J. From high-entropy ceramics to compositionally-complex ceramics: A case study of fluorite oxides. *J. Eur. Ceram. Soc.* **2020**, *40*, 2120–2129. [CrossRef]
8. Catalan, G.; Scott, J.F. Physics and Applications of Bismuth Ferrite. *Adv. Mater.* **2009**, *21*, 2463–2485. [CrossRef]
9. Yakout, S.M. Spintronics and Innovative Memory Devices: A Review on Advances in Magnetoelectric $BiFeO_3$. *J. Supercond. Nov. Magn.* **2021**, *34*, 317–338. [CrossRef]
10. Basu, S.; Hossain, S.K.M.; Chakravorty, D.; Pal, M. Enhanced magnetic properties in hydrothermally synthesized Mn-doped $BiFeO_3$ nanoparticles. *Curr. Appl. Phys.* **2011**, *11*, 976–980. [CrossRef]
11. Liu, Y.; Tan, G.; Guo, M.; Chai, Z.; Lv, L.; Xue, M.; Ren, X.; Li, J.; Ren, H.; Xia, A. Multiferroic properties of La/Er/Mn/Co multi-doped $BiFeO_3$ thin films. *Ceram. Int.* **2019**, *45*, 11765–11775. [CrossRef]
12. Dai, W.; Li, Y.; Jia, C.; Kang, C.; Li, M.; Zhang, W. High-performance ferroelectric non-volatile memory based on La-doped $BiFeO_3$ thin films. *RSC Adv.* **2020**, *10*, 18039–18043. [CrossRef] [PubMed]
13. Sen, A.; Hasan, M.K.; Munna, A.H.; Roy, D.J.; Al Hassan, M.R.; Gulshan, F. Structural, optical, and magnetic properties of compositionally complex bismuth ferrite ($BiFeO_3$). *J. Mater. Sci. Mater. Electron.* **2020**, *31*, 19713–19727. [CrossRef]
14. Suresh, P.; Hazra, B.K.; Kumar, B.R.; Chakraborty, T.; Babu, P.D.; Srinath, S. Lattice effects on the multiferroic characteristics of (La, Ho) co-substituted $BiFeO_3$. *J. Alloys Compd.* **2021**, *863*, 158719. [CrossRef]
15. Kirsch, A.; Bøjesen, E.D.; Lefeld, N.; Larsen, R.; Mathiesen, J.K.; Skjærvø, S.L.; Pittkowski, R.K.; Sheptyakov, D.; Jensen, K.M.Ø. High-Entropy Oxides in the Mullite-Type Structure. *Chem. Mater.* **2023**, *35*, 8664–8674. [CrossRef] [PubMed]
16. Wang, Y.; Robson, M.J.; Manzotti, A.; Ciucci, F. High-entropy perovskites materials for next-generation energy applications. *Joule* **2023**, *7*, 848–854. [CrossRef]
17. Yeh, J.W.; Chen, Y.L.; Lin, S.J.; Chen, S.K. High-Entropy Alloys—A New Era of Exploitation. *Mater. Sci. Forum* **2007**, *560*, 1–9. [CrossRef]
18. Ameer, Z.; Monteduro, A.G.; Rizzato, S.; Caricato, A.P.; Martino, M.; Lekshmi, I.C.; Hazarika, A.; Choudhury, D.; Mazzotta, E.; Malitesta, C.; et al. Dielectrical performance of high-k yttrium copper titanate thin films for electronic applications. *J. Mater. Sci. Mater. Electron.* **2018**, *29*, 7090–7098. [CrossRef]
19. Monteduro, A.G.; Rizzato, S.; Leo, C.; Karmakar, S.; Sirsi, F.; Leo, A.; Tasco, V.; Esposito, M.; Passaseo, A.; Caricato, A.P.; et al. Dielectric and Ferroelectric Response of Multiphase Bi-Fe-O Ceramics. *Phys. Status Solidi (A)* **2019**, *216*, 1800584. [CrossRef]
20. Monteduro, A.G.; Ameer, Z.; Martino, M.; Caricato, A.P.; Tasco, V.; Lekshmi, I.C.; Rinaldi, R.; Hazarika, A.; Choudhury, D.; Sarma, D.D.; et al. Dielectric investigation of high-k yttrium copper titanate thin films. *J. Mater. Chem. C Mater.* **2016**, *4*, 1080–1087. [CrossRef]
21. Monteduro, A.G.; Ameer, Z.; Rizzato, S.; Martino, M.; Caricato, A.P.; Tasco, V.; Lekshmi, I.C.; Hazarika, A.; Choudhury, D.; Sarma, D.D.; et al. Investigation of high-k yttrium copper titanate thin films as alternative gate dielectrics. *J. Phys. D Appl. Phys.* **2016**, *49*, 405303. [CrossRef]
22. Zhou, S.; Pu, Y.; Zhang, Q.; Shi, R.; Guo, X.; Wang, W.; Ji, J.; Wei, T.; Ouyang, T. Microstructure and dielectric properties of high entropy $Ba(Zr_{0.2}Ti_{0.2}Sn_{0.2}Hf_{0.2}Me_{0.2})O_3$ perovskite oxides. *Ceram. Int.* **2020**, *46*, 7430–7437. [CrossRef]
23. Yang, B.; Liu, Y.; Lan, S.; Dou, L.; Nan, C.W.; Lin, Y.H. High-entropy design for dielectric materials: Status, challenges, and beyond. *J. Appl. Phys.* **2023**, *133*. [CrossRef]
24. Fan, L.; Li, Y.; Li, J.; Xiang, Q.; Wang, X.; Wen, T.; Zhong, Z.; Liao, Y. High entropy dielectrics. *Open Access J. Adv. Dielectr.* **2023**, *13*, 2350014. [CrossRef]
25. Xie, H.; Li, J.; Yang, S.; Wu, L.; Li, P.; Qi, X. Microstructures and dielectric properties of novel $(La_{0.2}Pr_{0.2}Nd_{0.2}Sm_{0.2}Eu_{0.2})_2Ce_2O_7$ high entropy ceramics. *J. Mater. Sci. Mater. Electron.* **2021**, *32*, 27860–27870. [CrossRef]
26. Suresh, P.; Srinath, S. Study of structure and magnetic properties of rare earth doped $BiFeO_3$. *Phys. B Condens. Matter* **2014**, *448*, 281–284. [CrossRef]